Near-Field vs Far-Field Stratification Dynamics in Multi-Jet Hydrogen Combustors

Avighna Daruka

IB1

Oslo International School

Contents

1 Introduction

1.1 Background and Motivation

1.1.1 Aviation's Climate Challenge and Hydrogen as an Alternative

Currently, the aviation industry contributes approximately 2-3% of global carbon dioxide emissions, a value expected to triple by 2050 [1] as air travel becomes more accessible and demand increases. To combat this, hydrogen powered aircraft have emerged as a promising alternative as they offer zero carbon emissions at the point of use and significantly reduced lifecycle greenhouse gas contributions when produced from renewable sources [2].

Hydrogen is now more important than ever as, unlike ground transportation where battery-electric vehicles offer a viable way to decarbonise, aviation faces fundamental physics constraints. Current commercial aircraft use Kerosene based fuels that have energy densities that current battery technology cannot provide. For example, a fully-electric Boeing 737 would need batteries weighing more than the maximum take-off weight of the entire aircraft.

This challenge has intensified research into alternative aviation fuels that can deliver the required energy density while eliminating carbon emissions. Hydrogen is especially promising as its gravimetric energy density (energy per kilogram) is approximately three times higher than kerosene-based jet fuel, which means that less fuel weight is needed for the same flight range [2].

However, hydrogen's extremely low density as a gas creates storage challenges as even when liquefied at -253°C, hydrogen occupies roughly four times the volume of an equivalent energy content of jet fuel. Despite these engineering obstacles, major aerospace manufacturers including Airbus, Boeing, and Rolls-Royce have committed to hydrogen-powered aircraft development, with Airbus targeting commercial hydrogen aircraft entry into service by 2035 [3]. Therefore the future of Hydrogen looks promising.

1.1.2 Hydrogen Combustion Fundamentals and Challenges

Hydrogen combustion differs fundamentally from conventional hydrocarbon fuels in ways that directly impact combustor design and research methodologies. Understanding these differences is essential for interpreting the mixing and stratification behaviour investigated in this study.

Firstly, Hydrogen reacts with oxygen at a rate that is extraordinarily faster than kerosene or methane. The laminar flame speed of hydrogen is approximately 1.85 m/s at stoichiometric conditions, which is approximately four times higher than methane (0.45 m/s) [4]. In practice, this means that once hydrogen and air are mixed together, the chemical reactions occur almost instantaneously at combustion temperatures. Therefore, and crucially, the rate of combustion in my Hydrogen combustor is not limited by how quickly chemical reactions can happen, but rather how quickly air and fuel can mix together.

This phenomenon is coined being mixing limited, and is the fundamental assumption underlying this entire study.

Along with its high laminar flame speed, Hydrogen can also burn in air across a wide range of mixture compositions. This wide flammability range means that combustors must maintain stable combustion even when local fuel-air ratios vary significantly throughout. This increases the risk of unwanted combustion in regions where fuel and air are not well mixed, potentially leading to hot spots, flashback (flame propagating upstream into injectors, possible causing an explosion), or unstable operation (which will lead to numerical divergence).

Finally, Hydrogen is also known for having low ignition energy and high flame temperature. Specifically, Hydrogen requires only 0.02 millijoules to ignite (which is approximately one-tenth the energy needed for hydrocarbon fuels), this means that, in the combustor, hydrogen can auto-ignite under conditions that would normally be safe. This necessitates the careful control of temperature and mixture composition near injection points to prevent premature ignition before fuel and air are properly mixed.

Overall, these fundamental properties mean that the combustor performance is dominated by mixing quality rather than reaction kinetics. How uniformly fuel and air mix, and how this mixing evolves along the combustor length, directly determines combustion efficiency, temperature uniformity, and emissions. This is why stratification (non-uniform mixing) becomes the central focus of this research.

1.1.3 The Role of Mixing in Combustor Performance

The mixing of the fuel and air fundamentally determine three crucial aspects of combustor performance:

1. **Combustion Efficiency:** In the scenario of perfect mixing, a uniform fuel-air mixture would be created throughout the flow domain. This would theoretically allow all the fuel moleculues to find sufficient oxygen for complete combustion. In reality, imperfect mixing creates regions whee the mixture is either too fuel-rich, or too fuel-lean. Fuel-rich regions would create regions which have incomplete combustion and unburnt hydrogen that exists the combustor. Fuel-lean regions on the other hand would create regions with no combustion at all, which would also reduce combustion efficiency. Therefore, we can infer that an increase in mixing quality would correlate with improved efficiencies.

2. **Species Distribution:** The spatial distribution of combustion products, namely H_2O, would serve as a direct indicator of where combustion occured. Regions with high H_2O concentration would indicate areas where fuel and air mixed well and reacted completely. Conversely, regions with low H_2O would indicate poor mixing or incomplete combustion. This is therefore another parameter I track.

3. **Emissions Control:** For hydrogen combustion, the primary emission concern

would be nitrogen oxides formed when atmospheric nitrogen (N_2) reacts with oxygen in the air at temperatures above approximately 1800 K. The NO_x formation rate increases exponentially with temperature, which means that hot combusting areas could serve as high emission release points. Achieving low NO_x emissions would require maintaining uniform, moderate temperatures throughout the combustor. This is a direct result of optimum mixing. However, in the non-premixed combustion model used, I did not explicitly solve for NO_x formation kinetics. The focus of this study is therefore on characterizing the underlying mixing and temperature distribution patterns that determine where NO_x would form, rather than predicting absolute emission levels.

Overall, given these critical relationships between mixing quality and combustor performance, undersanding how mixing evolves along the combustor becomes quintessential. This study specifically investigates stratification, which characterises the non-uniformity of the fuel-air mixture and how it changes from the injection region (near-field) to the downstream combustor (far-field). By quantifying stratification behaviour in these two regimes and understanding the physical mechanisms behind them, I aim to correlate mixing efficiency with key flow variables. This information can then be used to recommend design strategies to optimize mixing quality and enhance overall combustor performance.

1.2 Stratification in Non-Premixed Combustion

1.2.1 Defining Stratification

In non-premixed combustion systems, the fuel and oxidiser are introduced separately and mix mainly through turbulent diffusion rather than prior homogenisation. As a result, the local fuel-air mixture composition varies significantly throughout the combustor, which is what gives rise to stratification. Stratification simply refers to the spatial non-uniformity of mixture composition, temperature, or combustion products within the flow field.

To quantitatively assess this behaviour, stratification must be described using a metric that will help capture net spatial variability in a physically meaningful and comparable manner. This motivates the definition of the Stratification Index (SI) introduced later in this work, which normalises local deviations and enables direct comparison across axial locations and operating conditions.

1.2.2 Using H_2O as a Proxy

Usually, in combustion research, stratification is most commonly quantified using the local equivalence ratio as it directly measures the relative proportions of fuel and oxidiser at each location. When the local species concentrations are well defined, the equivalence ratio provides an intuitive and widely accepted metric for measuring non-uniformity.

However, as I am using a non premixed multi-jet combustor configuration, the direct use of local equivalence ratio presents significant limitations, particularly in the near-field

region. In this region, the hydrogen injectors extend into the combustor. As a result, large portions of the near-field contain regions where either fuel or oxidiser mass fractions dominate ($\rightarrow 1$). Under these conditions, the local equivalence ratio calculations approach zero or infinity depending on the sampling location, highly skewing results.

Therefore, for our case, the equivalence ratio would no longer represent meaningful mixing behaviour but instead reflect the influence of the injector. Consequently, the near-field equivalence ratio fields are not directly comparable to the far-field values, where turbulent diffusion has substantially homogenised the flow and local fuel–air ratios are well defined.

To overcome these challenges and to also make near-field and far-field values comparable, the mass fraction of water vapour (H_2O) is used as a proxy variable. Water is the primary stable product of hydrogen combustion, and its spatial distribution inherently integrates the effects of both mixing and reaction. Regions with higher H_2O mass fraction indicate locations where hydrogen and oxygen have mixed sufficiently to react, while low values indicate unmixed or weakly mixed zones.

Importantly, the H_2O produced would remain well-defined throughout the entire combustor domain, including the near-field injection region, allowing for a consistent and physically meaningful comparison of stratification behaviour between near-field and far-field mixing regimes.

1.2.3 Near-Field vs Far-Field Mixing Regimes

The evolution of stratification within the combustor is strongly dependent on axial position, as the flow transitions from being injector-controlled to turbulence-controlled. To capture this behaviour, the flow is separated into near-field and far-field mixing regimes.

The near-field regime would encompass the entire region immediately downstream of the injectors. Stratification levels here are therefore high but rapidly evolving, as strong velocity gradients would drive efficient turbulent mixing. Local mixture statistics in this region are highly sensitive to injection details and are not representative of global combustor behaviour.

Further downstream, the far-field regime is characterised by a more developed turbulent flow. Here, large-scale mixing has largely occurred. Stratification here would be likely caused due to the flame holding its own structure, and any unreacted H_2 alongside the walls.

Separating the flow into these two regimes allows for a physically meaningful interpretation of stratification dynamics. By analysing near-field and far-field behaviour independently, it becomes possible to distinguish rapid injector-driven homogenisation from slower downstream re-distribution processes, which is essential for understanding how mixing quality evolves along the combustor length.

1.3 Research Objectives

1.3.1 Primary Objective

The primary objective of this research is to quantify the evolution of stratification along the jet axis by employing H_2O mass fraction as a proxy for local mixture non-uniformity, and to distinguish between near-field and far-field mixing behaviour for various flow variables.

1.3.2 Secondary Objectives

The secondary objectives of this study are to:

1. Differentiate near-field and far-field mixing regimes
2. Quantify the effect of equivalence ratio ϕ on various flow variables
3. Quantify axial stratification separately for the near-field and far-field to assess the rate of mixing homogenisation
4. Examine the coupling between turbulence and stratification
5. Assess the suitability of H_2O as a proxy for mixture stratification, particularly in cases where the equivalence ratio calculation is impractical due to injector geometry and near-field distortion effects.

2 Theoretical Background

2.1 Hydrogen Combustion

2.1.1 Combustion Chemistry and Unique Flame Properties

In our combustor, the hydrogen combusts through a complex mechanism of several elementary reactions. The overall stoichiometric reaction for this combustion can be represented as follows,

$$2H_2 + O_2 + 3.76N_2 \rightarrow 2H_2O + 3.76N_2. \quad (1)$$

Here, nitrogen is treated as inert.

The stoichiometric air-to-fuel ratio (AFR) for hydrogen is approximately 34.32 by mass [5], significantly higher than that of hydrocarbon fuels[1].

[1]This value accounts for the stoichiometry between oxygen and hydrogen in a non-air mixture, as well as the air composition of 21% oxygen and 79% nitrogen by volume.

2.1.2 Equivalence Ratio Definition

In general, the equivalence ratio (ϕ) helps quantify the actual fuel-air mixture composition relative to the stoichiometric ratio required for complete combustion. It is defined as

$$\phi = \frac{(F/A)_{\text{actual}}}{(F/A)_{\text{stoich}}} \tag{2}$$

where F/A is the fuel-to-air mass ratio and AFR is the air-to-fuel ratio.

However, this form of the equivalence ratio is not appropriate for this study as we calculate in terms of mass flow.

Since the fuel-to-air ratio can be expressed in terms of mass flow rates:

$$\phi = \frac{\left(\frac{\dot{m}_{\text{fuel}}}{\dot{m}_{\text{air}}}\right)_{\text{actual}}}{\left(\frac{\dot{m}_{\text{fuel}}}{\dot{m}_{\text{air}}}\right)_{\text{stoich}}} \tag{3}$$

The stoichiometric fuel-to-air ratio is the reciprocal of the air-to-fuel ratio:

$$\left(\frac{F}{A}\right)_{\text{stoich}} = \frac{1}{AFR_{\text{stoich}}} \tag{4}$$

Substituting this relationship:

$$\phi = \frac{\dot{m}_{\text{fuel}}}{\dot{m}_{\text{air}}} \cdot AFR_{\text{stoich}} \tag{5}$$

Rearranging to solve for the required air mass flow rate as I hold the mass flow rate of fuel constant:

$$\dot{m}_{\text{air}} = \frac{\dot{m}_{\text{fuel}} \cdot AFR_{\text{stoich}}}{\phi} \tag{6}$$

For hydrogen combustion in air, $AFR_{\text{stoich}} = 34.3$. Additionally, $\dot{m}_{fuel}$ is held constant across all cases, therefore only $\dot{m}_{air}$ is varied as a boundary condition.

2.2 Mass Fraction Stratification

2.2.1 Stratificaton Index (SI) Definition

To quantify stratification, a Stratification Index (SI) is defined at each axial location z:

$$\text{SI}(z) = \frac{\sigma_Y(z)}{\bar{Y}(z)} \tag{7}$$

where:

- $\sigma_Y(z)$ is the standard deviation of the local mass fraction across all radial sampling points at axial position z,
- $\bar{Y}(z)$ is the mean mass fraction at that axial location.

Note that this is mathematically equivalent to the coefficient of variation (COV).

The standard deviation is calculated as:

$$\sigma_Y(z) = \sqrt{\frac{1}{N}\sum_{i=1}^{N}\left[Y_i(z) - \bar{Y}(z)\right]^2} \tag{8}$$

Here, N is the number of radial sampling points, and $Y_i(z)$ is the local mass fraction at radial position r_i.

A higher SI indicates stronger stratification, while SI values approaching zero indicate an almost homogeneous mixture.

2.2.2 Stratification Gradient $\frac{dY}{dr}$

In addition to the overall SI, it is useful to examine how the mass fraction changes along the radial direction. The radial stratification gradient is defined at each radial position as:

$$\frac{dY}{dr}\Big|_{i,z} = \frac{Y_{i+1}(z) - Y_{i-1}(z)}{r_{i+1} - r_{i-1}} \tag{9}$$

where i denotes the radial sampling index.

This discrete derivative (also known as the finite difference) captures the local rate of change of mass fraction from the combustor centreline towards the wall. By analysing both the SI and the radial gradient, I can characterise not only the overall degree of stratification but also how sharply the mixture composition varies within that axial location.

2.3 Governing Equations

The flow in the combustor is governed by the standard set of conservation equations for mass, momentum, energy, and chemical species. In this study, the flow is assumed to be steady and modelled using the Reynolds-Averaged Navier-Stokes (RANS) approach, which captures the effects of turbulence through averaging momentum. Radiation effects are included, but molecular diffusion is not explicitly, with turbulent mixing providing the dominant transport mechanism.

2.3.1 Mass Conservation (Continuity)

The continuity equation ensures mass conservation throughout the domain:

$$\nabla \cdot (\rho \mathbf{u}) = 0 \tag{10}$$

where ρ is the local density and $\mathbf{u}$ is the velocity vector. For compressible flows, ρ varies with temperature and composition; however, for moderate Mach numbers like what is being run here, the flow is often treated as weakly compressible.

2.3.2 Momentum Conservation (Navier-Stokes)

The momentum equation describes the forces on the fluid:

$$\rho(\mathbf{u} \cdot \nabla)\mathbf{u} = -\nabla p + \nabla \cdot (\mu_{\text{eff}} \nabla \mathbf{u}) + \rho \mathbf{g} \tag{11}$$

Here, p is the pressure, $\mathbf{g}$ is the gravitational acceleration, and $\mu_{\text{eff}} = \mu + \mu_t$ represents the effective viscosity, which includes molecular viscosity μ and turbulent viscosity μ_t from the RANS turbulence model.

2.3.3 Energy Conservation

The energy equation accounts for convective and diffusive transport, heat release from chemical reactions, and radiative energy transfer:

$$\nabla \cdot (\rho \mathbf{u} h) = \nabla \cdot (k_{\text{eff}} \nabla T) + \dot{q}_{\text{combustion}} + \dot{q}_{\text{radiation}} \tag{12}$$

where h is the specific enthalpy, k_{eff} is the effective thermal conductivity, and $\dot{q}_{\text{combustion}}$ and $\dot{q}_{\text{radiation}}$ are the volumetric heat release terms due to chemical reactions and radiation, respectively. Radiation is treated using the P-1 model in Fluent.

2.3.4 Species Conservation

The evolution of chemical species in the combustor is governed by the species conservation equation, which accounts for convection, turbulent mixing, and chemical reactions. For a species k, the equation can be written as

$$\frac{\partial(\rho Y_k)}{\partial t} + \nabla \cdot (\rho \mathbf{u} Y_k) = -\nabla \cdot \mathbf{J}_k + \dot{\omega}_k \tag{13}$$

where ρ is the density, Y_k is the mass fraction of species k, $\mathbf{u}$ is the velocity vector, $\mathbf{J}_k$ represents diffusive fluxes, and $\dot{\omega}_k$ is the net rate of production or consumption due to chemical reactions.

3 Computational Methodology

3.1 Combustor Geometry Design and Rationale

The computational domain that I used is an annular hydrogen-air combustor that has many features resembling a typical industrial combustor, including radial fuel injection and annular air inflow [6].

3.1.1 Geometric Specifications

The combustor consists of a cylindrical chamber with annular and radial air inlets and radial hydrogen injectors, as illustrated in Figure 1. The combustor dimensions were

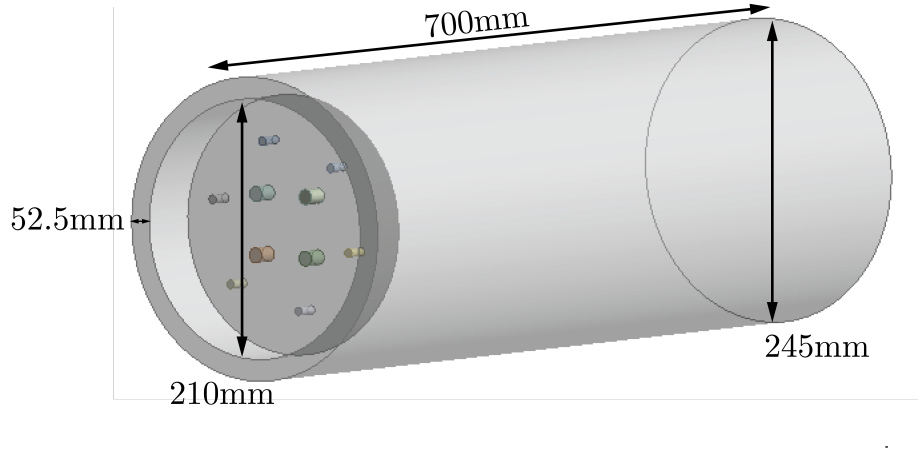

Figure 1: A front-on dimensioned view of the combustor used for the computational study.

selected based on three criteria:

- sufficient time for adequate hydrogen combustion to take place under 600 kW thermal power
- realistic length-to-diameter ratios representative of industrial gas turbine combustors
- a good trade off between mesh complexity, which would lead to longer case run times, and accuracy.

In the inlet of the combustor, I had an arrangement of fuel and air injectors, as illustrated in Figure 2.

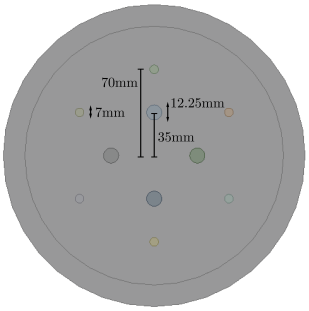

Figure 2: A cross-sectional view of the combustor inlet face.

3.1.2 Rationale

This fuel and air injector arrangement was selected primarily because it offered the best balance between combustion performance and accuracy, practical implications, and computational feasibility. Specifically, I had 4 radially arranged primary air injectors 35mm from the centre-line, 6 radially arranged fuel injectors 70mm from the centre-line, and an annular secondary-air inlet that was 105mm from the center-line (Figure 1).

This arrangement serves multiple purposes. Firstly, splitting flow between multiple injectors promotes enhanced fuel-air mixing while avoiding localized fuel-rich regions that could lead to autoignition [7] (the spontaneous ignition of hydrogen gas without a spark or flame [8]). Secondly, the symmetric distribution ensures uniform circumferential mixing, which helps maintain stable flame patterns. This also makes data analysis more accurate at specific radial positions.

This injector configuration is also representative of a modern lean-burn combustor design [9], albeit without swirlers or diffusers. This simplification was intentionally selected to isolate the effects of fuel injection arrangement and to allow for the investigation of equivalence ratio variations without the impact of inlet hardware geometry on the flow field.

The simplification was also considered due to the computational constraints from both the device used and the Ansys Fluent Software [10] (which has a 1M cell count limit for Student licenses). From a computational perspective, this arrangement provides sufficient geometric complexity to capture essential mixing and combustion phenomena while remaining manageable.

3.2 Meshing Strategy

As shown in Figure 3 I discretized the computational domain using a hexahedral meshing approach (conventional for such cases). Given the cylindrical geometry of the combustor and the circular cross-sections of the fuel and air injectors, this maintained high mesh quality and computational efficiency. As can be seen in the image, in the injection zone, the mesh was substantially refined further to capture the steep gradients in velocity, species concentration, and temperature. As shown in Figure 3(b), a high-density cell distribution surrounds each injector outlet, with progressive coarsening in the radial direction toward the outer wall. This radial refinement strategy ensures adequate resolution of the mixing layer while maintaining computational efficiency.

The final mesh consisted of 951575 elements and 972440 nodes. The element size for the cylindrical hexahedral region was 7.5mm, and the further refinement region had an element size of 5mm. I also ensured that the near-wall regions were resolved with sufficient refinement to capture boundary layer effects.

(a) A front on view of the mesh.

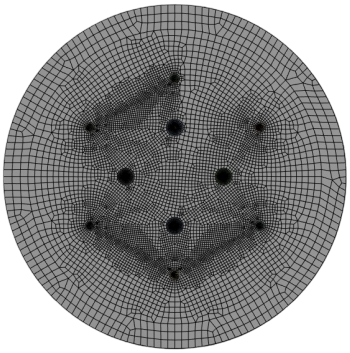

(b) The inlet face.

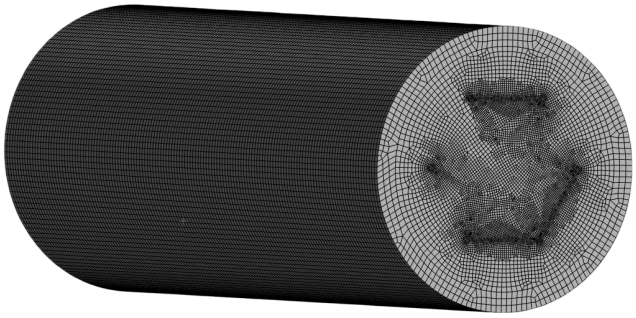

(c) The backside view of the mesh.

Figure 3: The computational mesh structure.

3.3 Boundary Condition Calculation

3.3.1 Fuel Inlet Condition

For all of my simulations, I kept the thermal input power constant at 600 kW. This power level was selected to be representative of a mid-scale gas turbine combustor used in combustion research [11]. This fixed thermal power led me to calculate a fixed hydrogen mass flow rate of

$$\dot{m}_{\text{fuel}} = \frac{\dot{Q}_{\text{input}}}{\text{LHV}_{H_2}} = \frac{600{,}000 \text{ W}}{119.96 \times 10^6 \text{ J/kg}} = 0.005002 \text{ kg/s}. \tag{14}$$

Here, the LHV_{H_2} of Hydrogen represents its Lower Heating Value [12], which is the amount of heat released by the complete combustion of the hydrogen when the water in the combustion products remains as a vapour, so the latent heat of vaporization is not recovered.

3.3.2 Outlet and Wall Conditions

The outlet of the combustor was specified as a pressure outlet boundary condition, with a gauge pressure set to a default 0 Pa (same as atmosphere). Setting the outlet as such allowed any flow to exit naturally, while also allowing me to record backflow, if any. This was especially important as the outlet was only 700mm away from the inlet, and therefore at low turbulent intensities[2] (around 5%) I was seeing backflow, which made me to tweak parameters (increase to 10%) to get physically meaningful results with the geometry I had. Therefore allowing the flow to exit naturally allowed me to bug-test any setup errors in my case.

In terms of walls, all solid surfaces (combustor walls and injector surfaces) were treated as no-slip adiabatic walls. The no-slip condition allowed me to see a realistic boundary layer through temperature contours, and also see how flow developed alongside the walls. The adiabatic assumption was used to simplify the thermal boundary treatment, as I wanted to primarily study internal mixing dynamics rather than wall heat transfer.

3.3.3 Species Transport

In my simulation, I modelled species transport and combustion through the Non-Premixed Combustion model in Ansys Fluent. This approach is especially well-suited for my current combustor configuration where the fuel and oxidizer are injected separately and mix through turbulent diffusion.

In Fluent, instead of tracking every individual gas species (H_2, O_2, H_2O, N_2) everywhere in the combustor, the model uses a simpler approach by tracking a single variable

[2]Turbulent Intensity is different from Turbulent Kinetic Energy as it is a relative measure of turbulence level expressed as a percentage of the mean flow velocity.

called the mixture fraction, which is a single scalar that represents the local mass fraction of fuel elements.

Other thermodynamic properties, such as temperature, species concentrations, and density are all calculated using a probability density function lookup table. This table takes into account turbulent fluctuations in the fluid by considering both the mean mixture fraction and how it varies. This was generated before running the simulation by solving detailed chemistry for different mixture fraction values beforehand, effectively incorporating turbulent fluctuations without the computational cost of solving detailed chemistry at every time step.

This approach is much faster than calculating chemical reactions at every point and every time step, which would require solving hundreds of reaction equations.

3.3.4 Energy and Radiation Model

Hydrogen combustion produces extremely hot flames (over 2000 K) with significant water vapour formation. At these temperatures, the hot gases emit thermal radiation which would transfer heat to cooler regions. Therefore, to model this radiative heat transfer, the P-1 radiation model was used.

Although the specifics of the model are outside the scope of the research, the P-1 model solves a simplified equation that tracks how the thermal radiation spreads through the combustor. While not as accurate as more complex radiation models, the P-1 model provides a good balance between accuracy and computational cost. Without accounting for radiation, the simulation would over-predict temperatures because it would ignore this heat loss mechanism.

Along with modelling radiation, the energy equation was also enabled to solve for temperature throughout the combustor. This equation accounts for heat released by combustion, heat transported by the flowing gases, and heat lost through radiation. Temperature prediction is critical because it affects reaction rates, gas density, and species concentrations.

3.3.5 Turbulence Modelling

Turbulence is a crucial parameter in studying the dynamics of stratification. Hydrogen flow in specific is highly turbulent due to the high-velocity jets from the fuel and air injectors. And therefore, a suitable turbulence model is critical.

Several turbulence models are available for CFD simulations, including the k-ϵ model (which is used for external flows), the Reynolds Stress Model (most accurate but computationally expensive), and the k-ω models. For this study, the k-ω SST (Shear Stress Transport) model was selected.

This model solves two additional equations:

- For turbulent kinetic energy (k): This represents the intensity of turbulent fluctuations [m^2/s^2]

- For specific dissipation rate (ω): This represents how quickly turbulent energy dissipates into heat [1/s]

This model was chosen specifically because it uses a blending function to switch between the k-ω in the near-wall region (which can capture the boundary layer in greater detail) and the k-ϵ in the free stream. This hybrid approach ensures accurate prediction of flow separation and mixing behaviour in the combustor without the free-stream sensitivity associated with a standard k-ω model.

3.3.6 Case Table

The main independent variable that was varied was the global equivalence ratio. This varied across lean to rich conditions while ensuring constant thermal power (600 kW). Table 1 shows the complete case matrix with corresponding boundary conditions.

Table 1: Simulation case matrix with inlet boundary conditions for all four cases.

Case ID	ϕ **(global)**	$\dot{m}_{\textbf{fuel,total}}$ **(kg/s)**	$\dot{m}_{\textbf{fuel,each}}$ **(kg/s)**	$\dot{m}_{\textbf{air,total}}$ **(kg/s)**	$\dot{m}_{\textbf{air,outer}}$ **(kg/s)**	$\dot{m}_{\textbf{air,inner}}$ **(kg/s)**
1	0.70	0.00500	0.000834	0.2452	0.1839	0.0153
2	0.85	0.00500	0.000834	0.2019	0.1515	0.0126
3	1.15	0.00500	0.000834	0.1493	0.1120	0.0093
4	1.45	0.00500	0.000834	0.1184	0.0888	0.0074

The specific equivalence ratio range of $\phi = 0.70$–1.45 was selected to span lean ($\phi < 1$), stoichiometric ($\phi \approx 1$), and moderately rich ($\phi > 1$) conditions. This range is representative of the typical operating conditions for real gas turbine combustors. Lean conditions ($\phi < 1$, which imply that there is more air than fuel) reduce NO_x emissions and therefore, are used for climate-aware combustors. Rich conditions ($\phi > 1$) ensure stable combustion but may lead to incomplete fuel burning [13]. The selected range allows for the investigation of how mixture composition affects stratification across different combustion regimes.

As shown in Table 1, the total fuel mass flow rate ($\dot{m}_{\text{fuel,total}} = 0.00500$ kg/s) was held constant across all cases. This fuel was distributed equally among 6 radial injectors, yielding $\dot{m}_{\text{fuel,each}} = 0.000834$ kg/s per injector. The air mass flow rate was adjusted according to Equation 6 to achieve the target global equivalence ratio. The total air flow was split between the annular outer ring and the 4 inner air injectors based on a 75-25% ratio. Note that this distribution is arbitrary.

3.4 Python Post-Process

After completing the simulations in Ansys Fluent, I extracted data at five axial locations (z = 25, 50, 150, 250, 350 mm) for post-processing and analysis. Raw simulation data was exported as Excel files, with each sheet corresponding to one axial position. From Fluent, I extracted mass fractions for H_2, O_2 and H_2O, static temperature, and Turbulent Kinetic Energy (TKE) and Turbulent Intensity.

I then developed a python script to automate the extraction and analysis of combustion data from the simulation results. The entire script and raw data can be found at the paper's Github repository. It can also be found in Appendix A.

A simple flowchart outlining the entire logic of the program is shown in Figure 4.

The workflow works by first importing the organised CFD simulation results from Excel, as outlined previously. Next, it separates the near-field and far-field axial values. For our study, I fixed this as the first two axial locations at 25 and 50mm representing the near-field, and the 150, 250, 350 mm axial locations representing the far-field.

After this , the stratification index (SI) is calculated at each radial point using central finite differences. The code iterates through all radial positions by computing local H_2O mass fractions and storing them for averaging in separate data-frames. The mean stratification gradient at each axial station is then determined using a simple arithmetic mean. Here, root-mean-squared approaches could be used, however since my data at every radial location is 1 dimensional in nature (as they are taken along a line), no value covers a greater area and therefore RMS would not necessarily be more accurate.

Finally, the code generates four plots and saves all the data into a separate excel file:

- Plot 1: SI vs axial distance
- Plot 2: TKE vs axial distance
- Plot 3 & 4: SI vs TKE for near-field and far-field data separately.

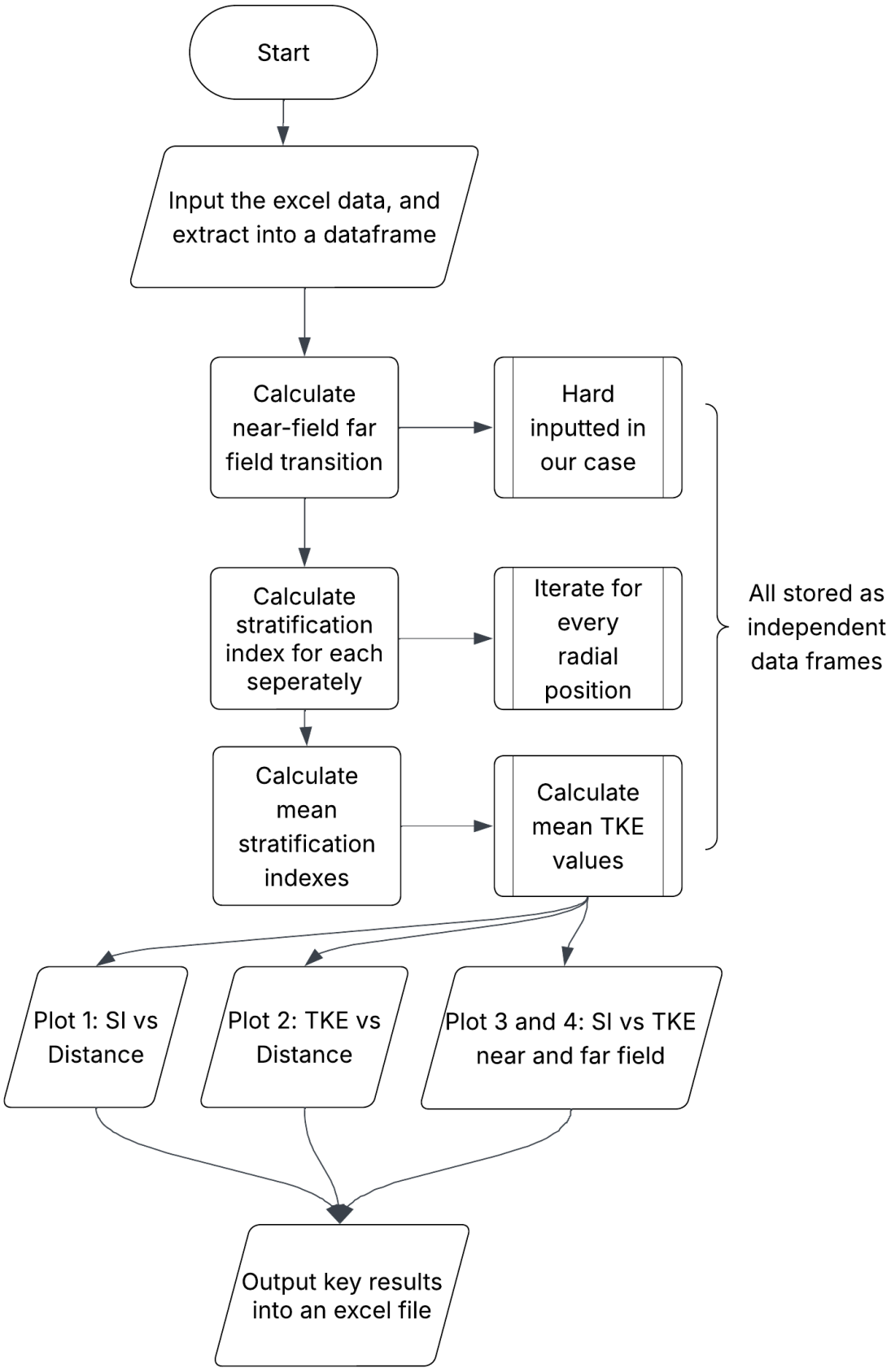

Figure 4: A flowchart outlining the entire flow of logic for the program used in post-processing.

4 Results and Post-Processing

4.1 Case Comparison Overview

Figure 5 and Figure 6 show the temperature and H_2O mass fraction contours for all four cases, ordered by increasing equivalence ratio. These contours show how fuel-air ratio affects flame structure, product distribution, and thermal patterns.

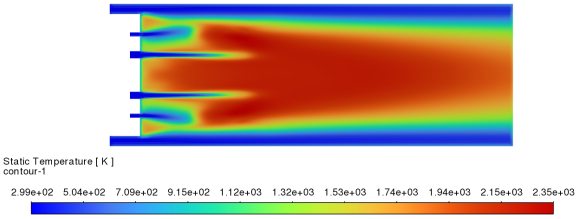

(a) Case 1: $\phi = 0.70$

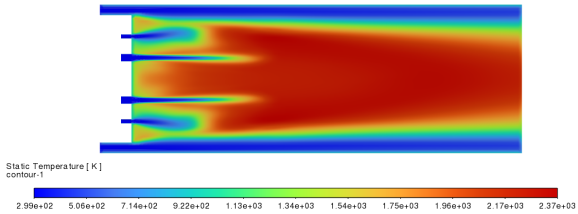

(b) Case 2: $\phi = 0.85$

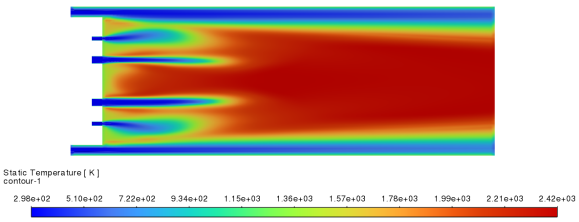

(c) Case 3: $\phi = 1.15$

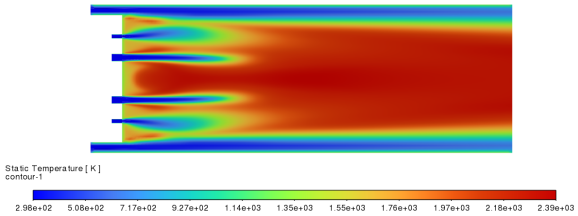

(d) Case 4: $\phi = 1.45$

Figure 5: Temperature field [K] for all four cases, ordered by increasing equivalence ratio.

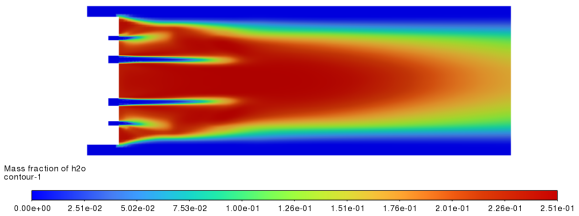

(a) Case 1: $\phi = 0.70$

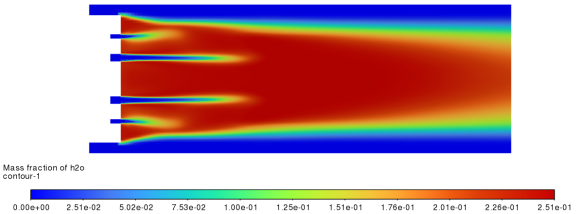

(b) Case 2: $\phi = 0.85$

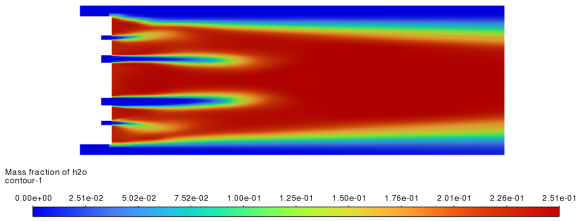

(c) Case 3: $\phi = 1.15$

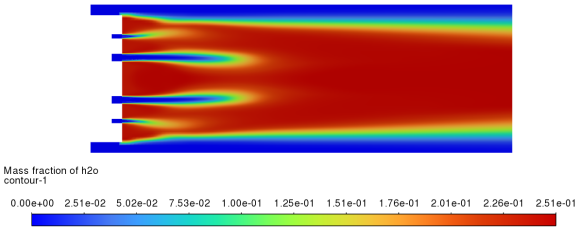

(d) Case 4: $\phi = 1.45$

Figure 6: H_2O mass fraction distributions for all four cases, showing the combustion product stratification patterns.

Figure 7 shows the turbulent kinetic energy (TKE) contours. TKE helps quantify the intensity of turbulent fluctuations that govern fuel-air mixing rates.

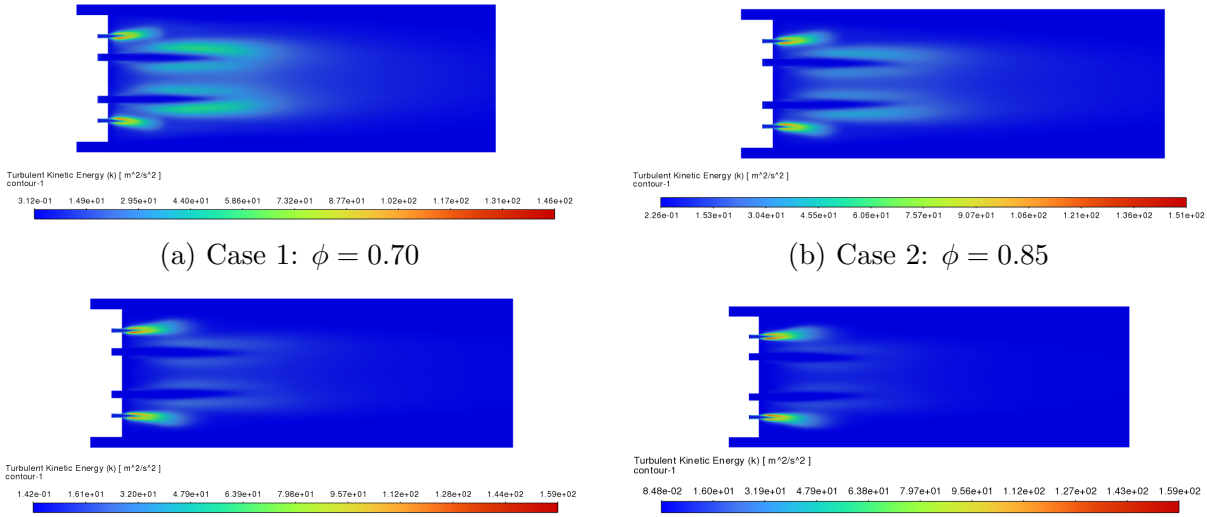

(a) Case 1: $\phi = 0.70$ (b) Case 2: $\phi = 0.85$

(c) Case 3: $\phi = 1.15$ (d) Case 4: $\phi = 1.45$

Figure 7: Turbulent kinetic energy [$\mathrm{m^2/s^2}$] distribution for all four cases.

4.1.1 Brief Analysis

For temperature, it can be seen how high-temperature zones are more concentrated near fuel injection points for cases with smaller ϕ values. As ϕ increases, the flame is also seen to increase in length, which is expected as high temperature zones would be spread out over a longer axial distance. This longer flame distance means that the boundary of the flame is more straight-on along the walls, this creates a more parallel flame structure in rich cases compared to the converging flame pattern seen in lean cases.

The H_2O mass fractions show similar trends to the temperature fields, with longer flame structures observed at higher equivalence ratios. The product distribution becomes more axially extended and parallel to combustor walls as ϕ increases. Near-wall regions consistently show low H_2O concentrations (<0.05) across all cases, which indicates that the secondary air remains largely unmixed with combustion products.

The TKE contours show that the maximum TKE values (40–80 m/s) occur at the fuel jet boundaries immediately downstream of injection, where the velocity gradients between high-speed hydrogen jets and air create intense shear layers [14]. TKE distributions show an inverse relationship with equivalence ratio. Lean cases show higher overall TKE levels compared to rich cases. This trend reflects the idea that since I hold $\dot{m}_{fuel}$ constant and vary $\dot{m}_{air,total}$, a higher equivalence ratio means less flow velocity for air, governed by the mass flow-velocity relationship

$$V_{air} = \frac{\dot{m}_{air}}{\rho_{air} A_{inlet}}.$$

Since $\phi \propto 1/\dot{m}_{air}$ for fixed fuel flow, increasing equivalence ratio directly reduces air mass flow rate and consequently air velocity.

4.2 Radial Evolution of Flow Variables

4.2.1 Plots

To study differences in the near-field and far-field of the combustor, I plotted radial profiles of temperature, hydrogen mass fraction, water mass fraction, and turbulent kinetic energy at two axial locations: z = 25 mm (near-field) and z = 350 mm (far-field). The near-field location captures the primary mixing zone immediately downstream of fuel injection, where jet-cross-flow interactions are most intense. The far-field location shows conditions approaching the combustor outlet, where the mixing processes have largely completed and the stratification patterns stabilize. The radial coordinate r = 0 corresponds to the combustor centreline, while r = 0.1225 m represents the outer wall boundary. These profiles show how equivalence ratio heavily influences various flow related parameters.

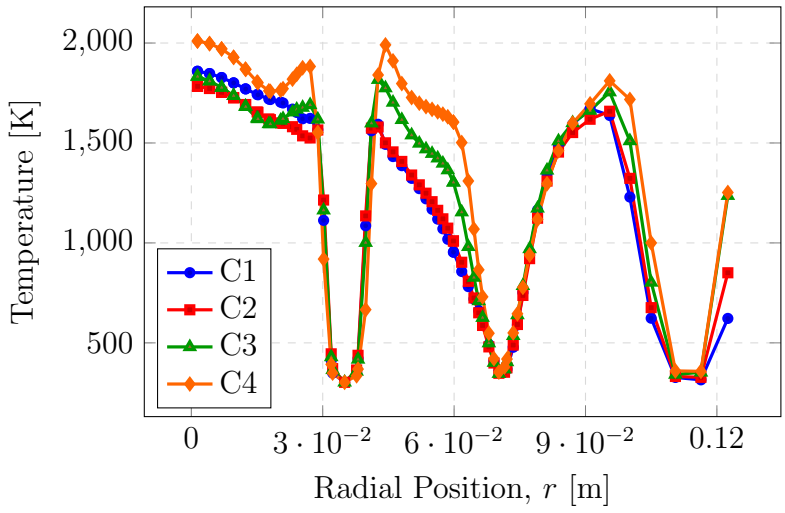

Figure 8: Radial Temperatures at z = 25 mm for all four equivalence ratio cases.

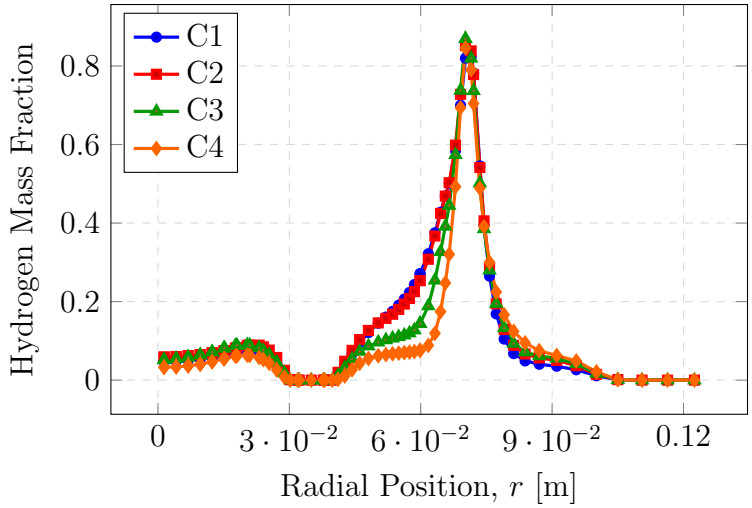

Figure 9: Radial Hydrogen mass fractions at z = 25 mm for all four equivalence ratio cases.

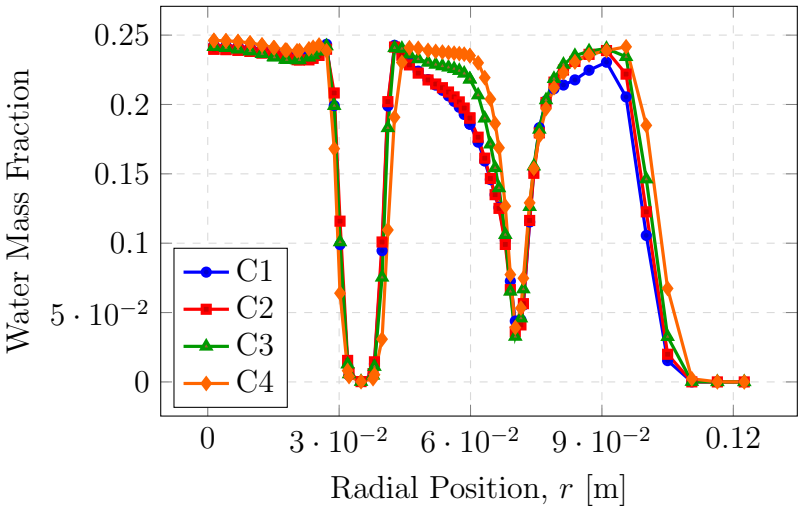

Figure 10: Water mass fractions at z = 25 mm for all four equivalence ratio cases.

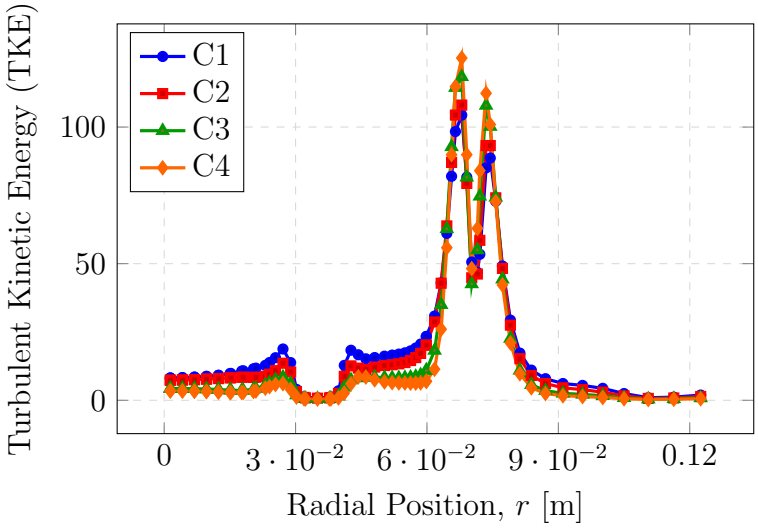

Figure 11: Turbulent Kinetic Energies at z = 25 mm for all four equivalence ratio cases.

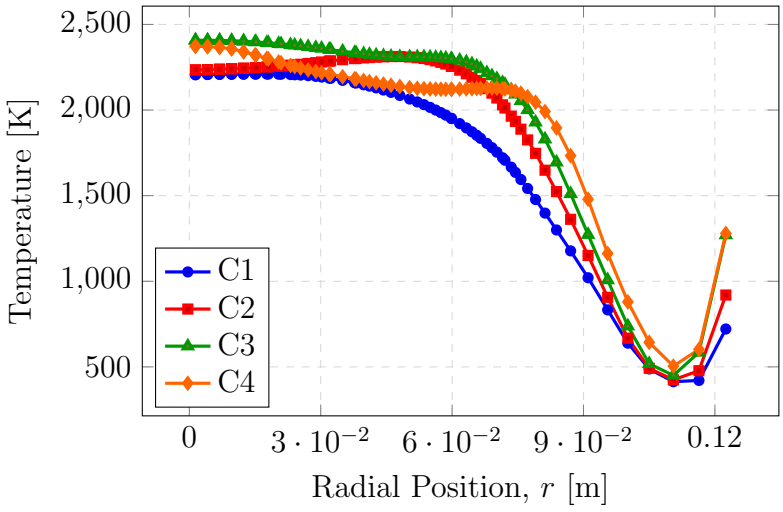

Figure 12: Radial Temperatures at z = 350 mm for all four equivalence ratio cases.

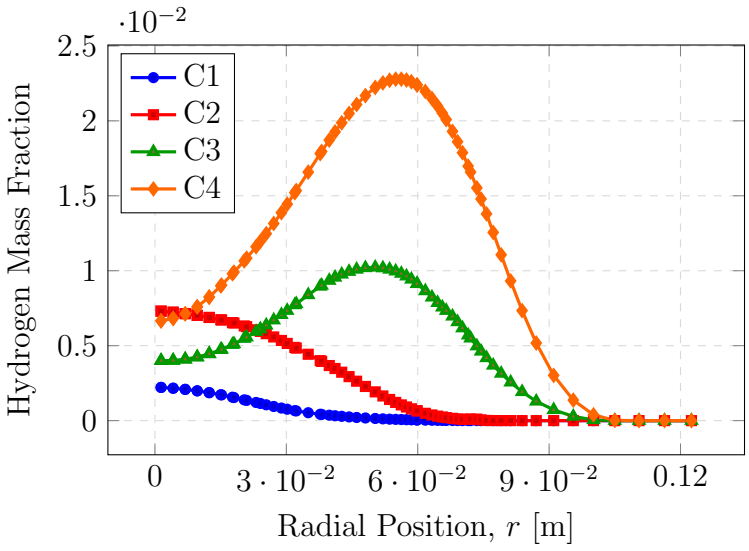

Figure 13: Radial Hydrogen mass fractions at z = 350 mm for all four equivalence ratio cases.

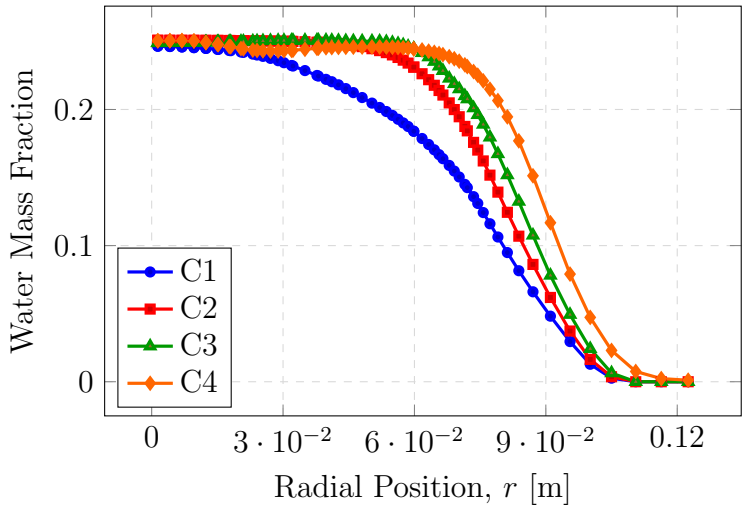

Figure 14: Water mass fractions at z = 350 mm for all four equivalence ratio cases.

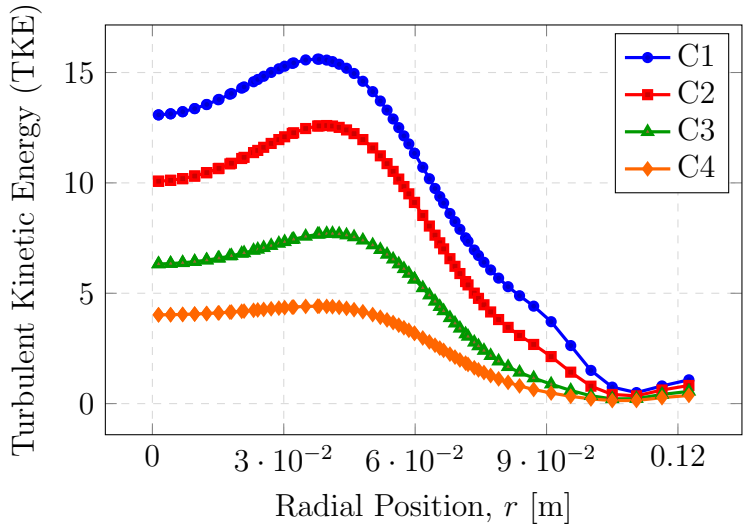

Figure 15: Turbulent Kinetic Energies at z = 350 mm for all four equivalence ratio cases.

4.2.2 Brief analysis

In terms of temperature, in the near-field, sharp drops can be seen in the fuel and air injector regions (r $\approx$ 0.03, 0.06, 0.09 m) with the temperatures ranging from 1700-2000K. Case 4 shows the highest peak temperature, as is expected for a greater fuel content. In the far-field, however, we see a more gradually varying profile compared to the multi-peaked near-field structure. Near the outer walls (r $\approx$ 0.09m) as was seen in the near-field case, we have a sudden drop in temperature. This can be verified by examining the temperature contours in figure 5. This is likely due to the unreacted annular air.

For hydrogen mass fraction, the near-field shows intense localization at the fuel injector, with peak values reaching 0.8-0.9. The lean cases (C1, C2) show broader H_2 peaks compared to the other cases, which indicate slower fuel consumption. In the far-field, the H_2 mass fractions are considerably lower, which confirms approximate total fuel consumption by z = 350 mm. However, Cases 3 and 4 show residual H_2 peaks of approximately 0.01 and 0.0225, respectively, at r $\approx$ 0.055 m. This is quite interesting as it indicates incomplete combustion in the richest operating condition due to excess fuel. The smooth profile shapes in the far-field demonstrate that turbulent mixing has eliminated the discrete jet structure.

The water mass fraction in the near-field shows several valleys at r $\approx$ 0.031, 0.07, 0.15 m. These correspond to fuel-rich zones where there is incomplete reactions. In the far-field, the distribution becomes much smoother with higher concentrations (0.22-0.25) in central regions that gradually decrease toward the walls. Case 1 shows the most gradual radial gradient, while the richer cases have steeper gradients. This persistent stratification can be observed in the water contour plots in Figure 6.

Finally, the TKE distributions in the near-field show intense turbulence production at fuel jet boundaries, and therefore has a similar shape to hydrogen mass fraction, with peak values reaching 100-120 m^2/s^2. In the far-field, the TKE values drop dramatically to 3-15 m^2/s^2, which is an almost 95% reduction from near-field peak values. Case 1 still has the highest far-field TKE ($\approx 15 m^2/s^2$), while the other cases are usually below TKE $\approx$ 10 m^2/s^2. The near-wall TKE ($r > 0.1$ m) remains minimal ($< 2\ m^2/s^2$) in both the near- and far-fields cases. This is likely due to viscous layer damping.

4.3 Axial Evolution of Flow Variables

Now I plotted the averaged values of temperature, H_2O mass fraction, H_2 mass fraction, and turbulent kinetic energy along all the tested axial positions to quantify the progression of combustion and mixing from inlet to outlet. This provides a global measure of combustion completion, product formation, and turbulence decay as flow develops through the combustor length.

4.3.1 Temperature and TKE Plots

The temperature and turbulent kinetic energy are plotted along the combustor axis to track the thermal development and turbulence. The vertical dotted line at z = 50 mm separates the near-field region, where intense mixing and combustion occur, from the far-field region, where flow properties approach outlet conditions.

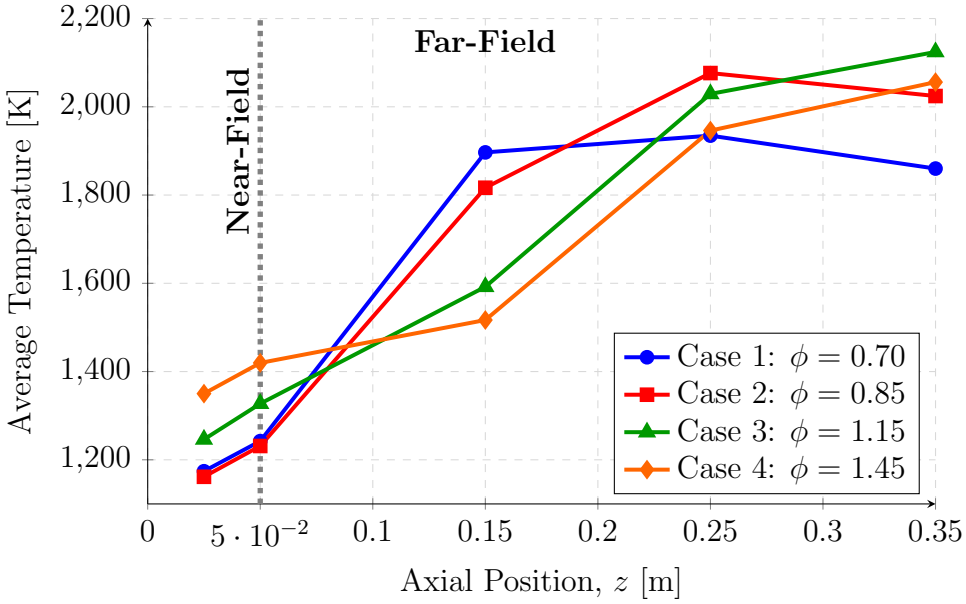

Figure 16: The temperature evolution along the combustor axis.

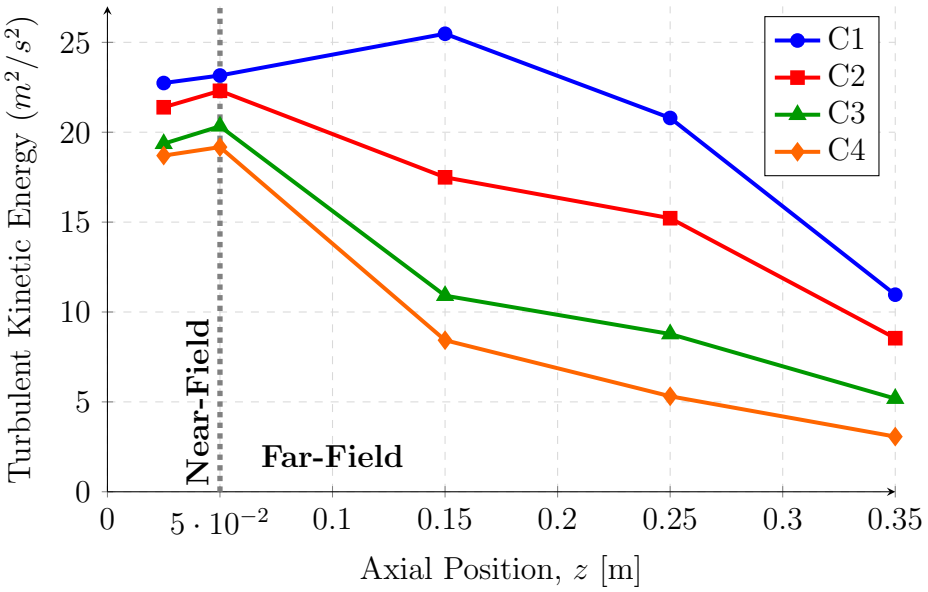

Figure 17: The TKE along the combustor axis.

The temperature can be seen increasing sharply through both the near-field and the far-field, rising from about 1160K to 2050K. Case 3 surprisingly has the highest far-field temperature, this could be a result of more complete fuel combustion by z=350mm compared to Case 4. Case 4 would likely have a higher temperature by the outlet.

TKE on the other hand decreases along the combustor for all cases. The clear ordering between cases ($C1 > C2 > C3 > C4$) shows the inverse relationship between equivalence ratio and air velocity, with lean operation producing stronger turbulence throughout due to higher air-velocities.

4.3.2 H_2O Stratification Index Axial Trends

Figure 18 illustrates the Stratification Index (SI) along the combustor axis for each case individually. The SI is calculated as the coefficient of variation of H_2O mass fraction across each radial profile at each axial location, quantifying the degree of product non-uniformity.

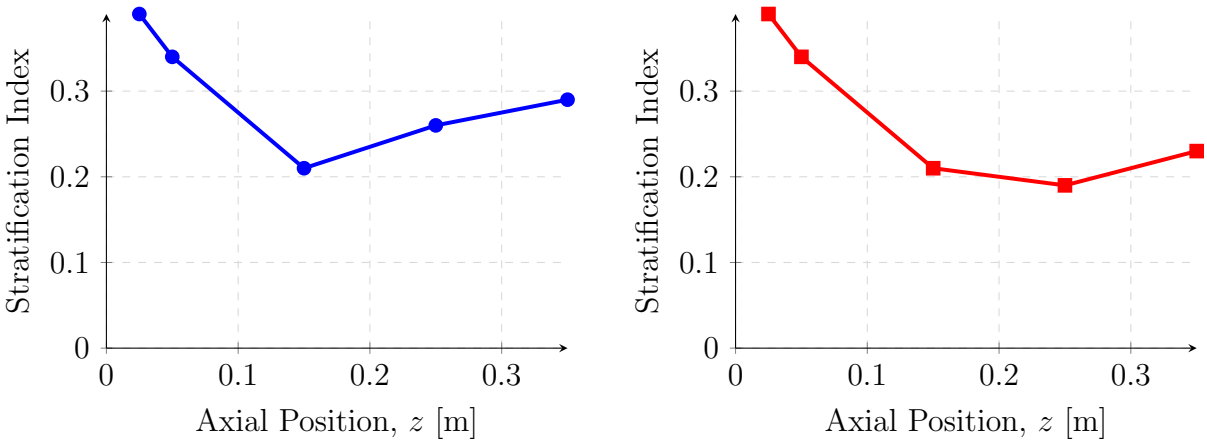

(a) Case 1: $\phi = 0.70$

(b) Case 2: $\phi = 0.85$

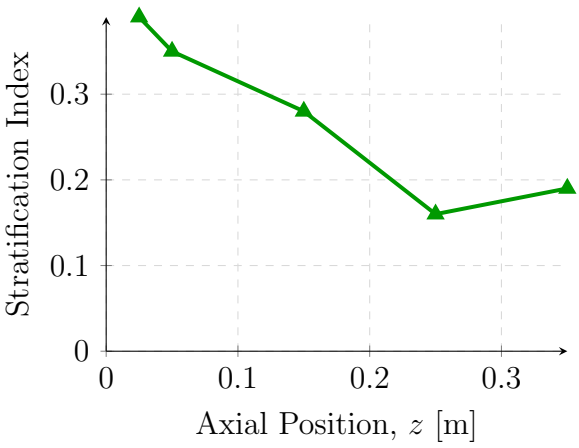

(c) Case 3: $\phi = 1.15$

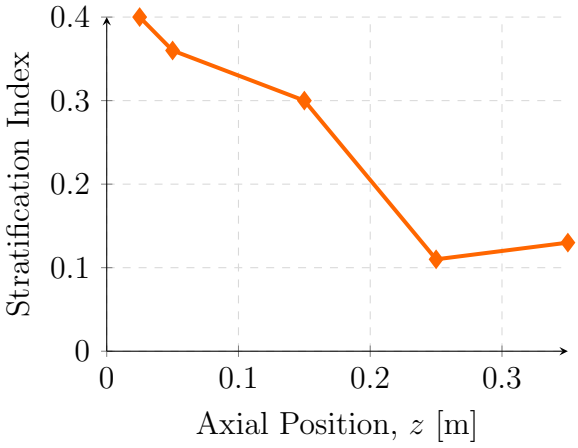

(d) Case 4: $\phi = 1.45$

Figure 18: Stratification Index evolution along the combustor axis for all four cases. All cases show initial decrease (mixing-driven homogenization) followed by increase in far-field (re-stratification).

All cases show a U-shaped trend. They can be seen decreasing from 0.36-0.40 at z = 25 mm to a minima at z = 150-250 mm, then increasing toward the outlet. This is clear evidence of near-field turbulent homogenization followed by far-field re-stratification. Case 1 (lean) reaches its minimum earliest and maintains a lower SI throughout, while the richer cases

show delayed minima and steeper far-field gradients. The outlet SI ranges from 0.13 (Case 4) to 0.29 (Case 1). This provides a key insight of how leaner cases mix faster but rich cases end up with lower SI values at the outlet, likely due to an extended flame length (as visible in Figure 5) which allows for greater mixing.

4.4 Turbulence-Stratification Coupling

4.4.1 Regime-Dependent SI-TKE Relationships

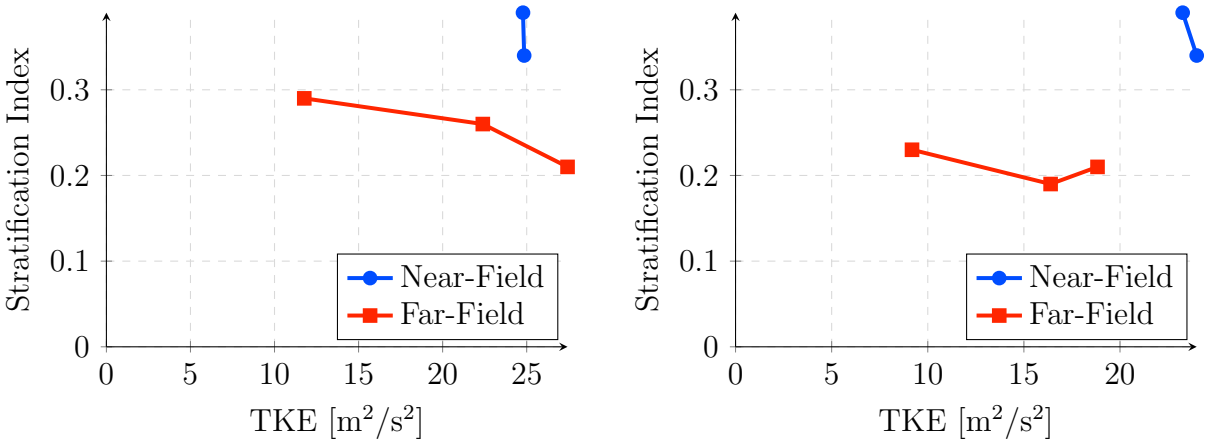

(a) Case 1: $\phi = 0.70$

(b) Case 2: $\phi = 0.85$

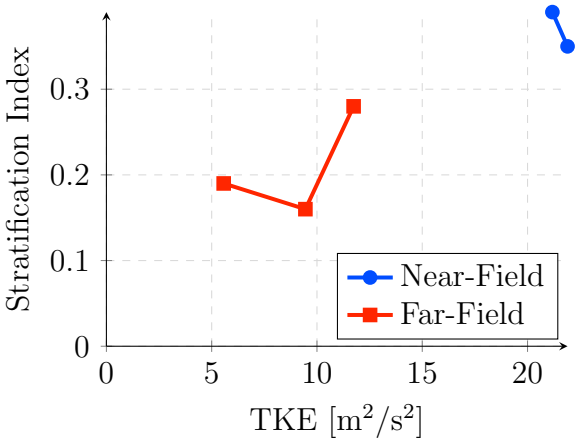

(c) Case 3: $\phi = 1.15$

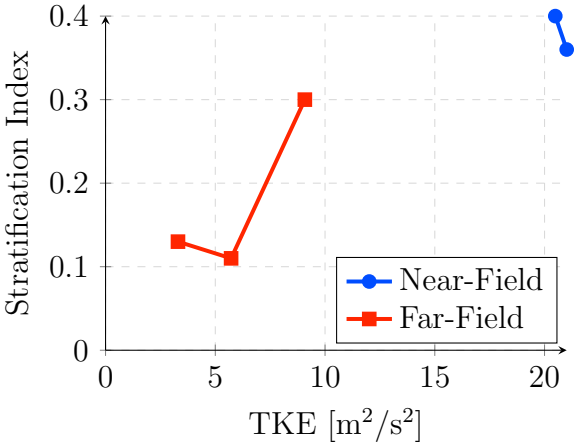

(d) Case 4: $\phi = 1.45$

Figure 19: Stratification Index vs Turbulent Kinetic Energy for all four cases.

Figure 19 shows the SI-TKE correlation plots. Across all 4 cases, we can see distinct near-field and far-field behaviour. Near field points in blue can be seen clustering at high TKE values of 18-25 m^2/s^2. These points exhibit minimal variation despite the turbulence range, which indicates that the initial stratification remains high regardless of turbulence intensity immediately after fuel injection.

The far-field points in red span a wider range of both TKE and SI. In Cases 1 and 2, far-field points have a weak negative correlation: as TKE decreases, the SI initially drops but then increases again. In Cases 3 and 4, this behaviour is stronger, forming

a U-shaped correlation. This behaviour is strong evidence for the competing effects of turbulent mixing (which reduces SI) and re-stratification (which increase SI).

5 Discussion

5.1 Physical Interpretation of Results

5.1.1 Near-Field Homogenisation

In the near-field, we can see rapid stratification reduction across all equivalence ratio cases, with the SI decreasing from initial values of 0.36-0.40 to 0.13-0.21 at z = 150-250 mm. This mixture homogenization is driven by turbulent mixing generated at the points where the fuel is injected. Evidence for this comes from Figure 11 where one can see that the points where TKE peaks (at roughly 0.3 and 0.5 m) maximum homogenisation takes place.

This behaviour is an example of jet-induced turbulent diffusion. Where the hydrogen fuel is injected, strong shear layers are created with the surrounding air streams. These shear layers generate turbulent eddies (which are created due to the friction between faster and slower moving fluid flows [15]) that break down concentration gradients through molecular diffusion. The radial profile of TKE in the far-field (Figure 15) shows smooth continuous distributions, which is direct evidence of turbulent homogenization.

Interestingly, the rate of near-field homogenization shows inverse dependence on equivalence ratio. Case 1 ($\phi = 0.70$) achieves its SI minimum earliest (z $\approx$ 150 mm) and has the steepest near-field gradient ($\frac{dSI}{dz} \approx -0.008 mm^{-1}$), while Case 4 ($\phi = 1.45$) shows us delayed homogenization with a shallower gradient ($\frac{dSI}{dz} \approx -0.004 mm^{-}1$). This trend directly correlates with TKE levels: leaner cases maintain higher TKE values (Figure 17) and higher air velocities which creates stronger turbulence and therefore faster mixing in the near-field.

5.1.2 Far-Field Re-stratification

Beyond the near-field, all cases show a stratification increase toward the combustor outlet. This is a counter-intuitive result given that turbulent mixing continues throughout the domain. Far-field gradients are mostly positive in the far-field for all cases. This re-stratification occurs despite the TKE decaying from peak values to 3-15 m^2/s^2 at z = 350 mm. We can therefore deduce that TKE is no longer the dominant mechanism, and therefore SI increases.

Instead of TKE, three physical mechanisms likely contribute to the re-stratification:

1. The H_2 mass fractions at 350mm in Figure 13 show us that there is a strong presence of residual unburned hydrogen in rich and lean cases at z = 350 mm. This indicates non-uniform combustion completion across the 4 cases. Regions where combustion

finishes early (see Figure 5) produce high H_2O concentrations and temperatures, while fuel-rich pockets with incomplete reactions result in low H_2O concentrations near the walls, which directly leads to increased stratification. This observation is further supported by the extended flame lengths visible in the temperature contours of the rich cases in Figure 5.

2. Along with residual fuel, the temperature profiles at z = 350 mm (Figure 12) show hot cores (1800-2200 K) and cooler near-wall regions (800-1200 K). This radial thermal gradient can induce secondary flows [16] (akin to convection) that can redistribute H_2O non-uniformly.

3. The SI-TKE plots in Figure 19 show U-shaped far-field trajectories. It can be seen that as TKE decreases from 15 m^2/s^2 to 3 m^2/s^2, SI initially decreases (which means that turbulent mixing is still effective) then increases (which means thermal stratification then likely dominates). This suggests a critical TKE threshold (5-8 m^2/s^2) below which re-stratification dominates[3].

5.1.3 The Effects of Equivalence Ratio

The equivalence ratio has opposing effects on near-field and far-field stratification. In lean cases, we see rapid near-field homogenization but higher outlet SI (e.g. 0.29 in Case 1), while rich cases have slower initial mixing but lower final SI. This crossover is evidence for fundamentally different controlling mechanisms in each regime.

In the near-field, air velocity dominates mixing quality. For a fixed fuel flow ($\dot{m_{fuel}}$ = 0.005 kg/s), lean cases require have a higher air mass flow ($\dot{m_{air}}$ = 0.245 kg/s for ϕ = 0.70 vs. 0.118 kg/s for ϕ = 1.45). This produces proportionally higher jet velocities and TKE (24 vs. 18). This 33% increase in TKE increase causes steeper stratification gradients through enhanced turbulent diffusion gradients, as discussed.

In the far-field, the flame length becomes crucial. The rich cases have much more extended reaction zones which provide additional axial distance for turbulent mixing before flow exits. Lean cases complete combustion earlier, which doesn't allow for further mixing.

The optimal equivalence ratio for minimizing outlet stratification appears to be moderately rich ($\phi \approx$ 1.15-1.45), where the extended flame length compensates for initially weaker mixing. However, this comes at the cost of incomplete fuel consumption (Figure 13) and potentially higher thermal NO_x emissions due to higher temperatures (Figure 12). This can be addressed by altering combustor geometry.

[3]Note that this value is highly sensitive to combustor geometry and initial conditions, and therefore cannot be generalised.

5.2 Comparison with Literature

5.2.1 Novel Contribution by using H_2O as Stratification Proxy

Most stratification studies use the local equivalence ratio (ϕ_{local}) as the primary metric for stratification. Although this is intuitive, this approach becomes hard to implement in multi-jet geometries as the near-field would capture both pure fuel or pure air regions ($\phi \to \infty$) or ($\phi \to 0$), which produces numerically unstable SI calculations.

My use of H_2O mass fraction as a stratification proxy avoids this limitation. Unlike ϕ_{local}, which requires well-mixed fuel-air mixtures, the H_2O mass fraction remains well-defined everywhere: zero in unmixed regions, non-zero only where the reaction occurred. This makes my SI calculations easily comparable between near-field and far-field regimes, an advantage for multi-injector-combustor analysis.

A potential limitation of this method is that this SI value equates mixing quality with combustion completion. In the far-field, a high SI could indicate either poor mixing or incomplete reaction (fuel and air mixed but didn't burn). The residual H_2 suggests that both likely occurred, however distinguishing would require species decomposition that is beyond this study's scope.

5.2.2 Differences from Premixed Combustion Behavior

Most studies of premixed combustion [17] show that usually stratification strictly decreases as the flame propagates downstream. My non-premixed configuration shows the opposite behaviour as stratification is seen increasing downstream. This is a novel finding unique to current literature.

This difference highlights a key limitation of applying classical premixed stratification theory to non-premixed systems. In non-premixed flames such as mine, the mixture composition actively changes through mixing and reaction, creating stratification patterns that are absent from inlet conditions. The U-shaped SI curves are a signature of this coupling, a phenomenon that would be impossible in premixed systems where SI can only decrease.

5.3 Limitations and Sources of Uncertainty

5.3.1 Computational Model Limitations

My non-premixed combustion model assumes that the reaction happens instantaneously (which, for hydrogen, it nearly does), which may over predict the reaction rates. Chemistry with more finite-rates would be more more accurate, and give better temperature predictions, but it would be at 10-100x the computational cost.

The $k-\omega$ SST turbulence model that I used is an example of a Reynolds-Averaged Navier-Stokes (RANS) approach that averages turbulent fluctuations. Large Eddy Simulation (LES) would instead solve for instantaneous turbulent structures and therefore

provide superior mixing predictions, particularly for unsteady phenomena the used fuel jets. However, LES requires 100x finer meshes and was computationally infeasible within the 1M cell limit of the Student Fluent License I was using.

Lastly, the adiabatic wall boundary condition does not take into account heat loss to the combustor walls, which in real systems would reduce near-wall temperatures and potentially change the observed stratification patterns. This is especially important as the re-stratification that I saw was partly due to the cold un-burnt fuel at the walls. Heat transfer simulations would address this limitation but again it would exceed the available computational resources[4].

5.3.2 Uncertainty in Stratification Metrics

The stratification metrics are calculated from only 5 axial locations, which is a rather coarse axial resolution. A denser axial sampling (10 mm spacing for example) would improve the transition accuracy of near-field and far-field, but would require re-running simulations with more frequent data extraction[5].

The choice of radial sampling strategy also affects the SI values. The data was extracted along a single radial line rather than circumferentially averaged profiles. For a perfectly symmetric combustor such as the one used in this study, these should be equivalent, but asymmetry between the two definitely introduces variation. Ideally, the SI would be computed from multi-line sampling, which was not performed due to post-processing complexity.

5.4 Combustor Design Implications

Based on the data collected, we can infer several design trade-offs that can be used for hydrogen combustor optimisation. A stratification surface outlining these trade-offs is illustrated in Figure 20.

Figure 20 shows the heavily non-linear relationship between axial mixing and equivalence ratio. The surface has a prominent valley with SI $\approx$ 0.11-0.16 at z = 150-250 mm for rich operating conditions $\phi > 1.15$. This region represents the place where turbulent homogenisation has completed, as beyond, stratification increases. The sharp decrease in SI leading up to this valley further demonstrates the rapid near-field mixing driven by turbulence, while the subsequent gradual ascent toward the outlet shows the re-stratification as TKE decreases. The downward slope seen from lean to rich conditions also confirm that higher equivalence ratios produce lower absolute stratification throughout the combustor.

This three-dimensional view can enable combustor designers to directly identify optimal operating points. For example, if one wants to make a compact combustor (z $<$ 150 mm), the optimum choice would be lean operation that leverages faster initial mixing despite higher outlet stratification. Conversely, for longer combustors (z = 200-250 mm),

[4]Which are limited to a Macbook Pro.

[5]For reference, each simulation took about 5 hours to run. x30 for this study.

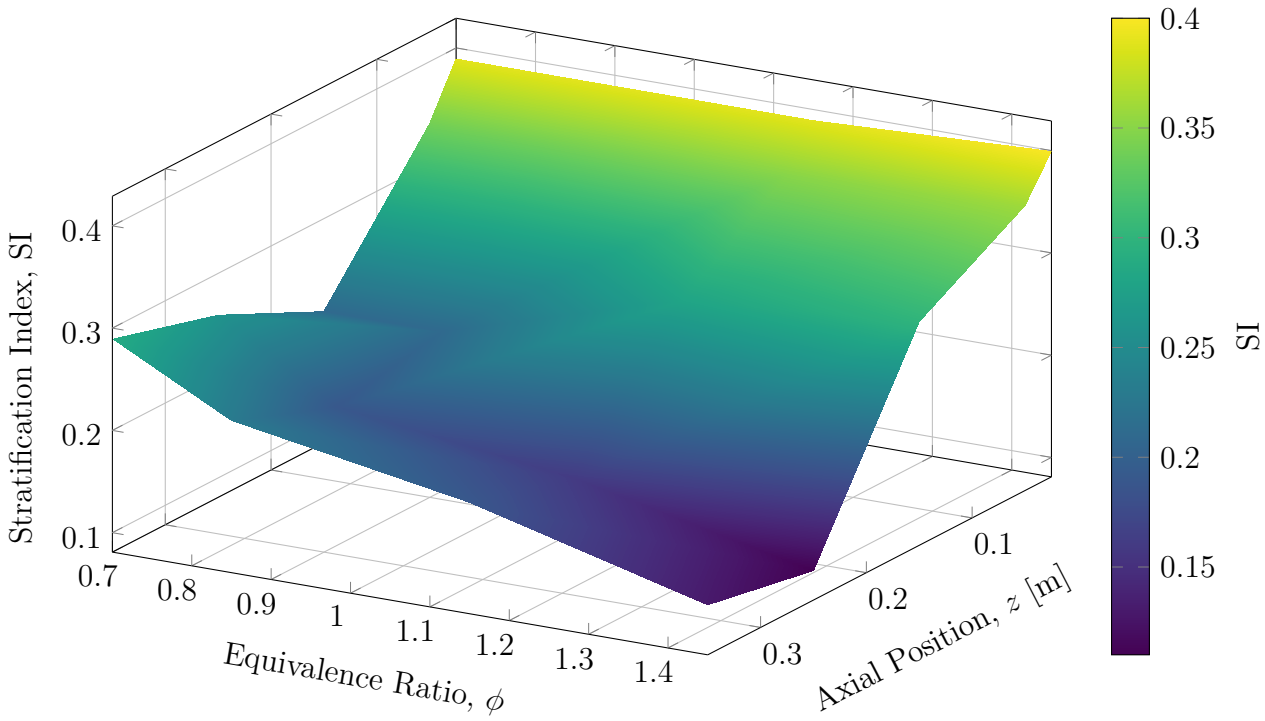

Figure 20: A three-dimensional stratification landscape showing SI as a function of axial position and equivalence ratio. The surface has a valley at z ≈ 150-250 mm, with re-stratification occurring downstream.

rich operation would be beneficial to minimize exit stratification. The smooth gradient structure indicates that any intermediate equivalence ratios would provide continuously varying performance. This allows for combustor designers to fine-tune parameters according to their specific use cases.

6 Conclusion

This paper successfully quantified radial stratification dynamics in hydrogen multi-jet combustors across various equivalence ratios of 0.70-1.45 using H_2O mass fraction as a proxy for mixture non-uniformity. All cases showed a characteristic U-shaped stratification evolution where rapid near-field homogenization caused by turbulence was followed by far-field re-stratification as turbulent kinetic energy decreased. Lean operation ($\phi = 0.70$) produced faster initial mixing due to higher air velocities and turbulence levels, but also led to higher outlet stratification, while rich conditions ($\phi = 1.45$) showed delayed homogenization but achieved lower final stratification because of extended flame length. The turbulence-stratification coupling analysis showed unique regime-dependent behaviour: strong negative correlation in the near-field and U-shaped far-field relationships indicated a critical TKE threshold (≈ 5-8 m^2/s^2) below which thermal re-stratification dominates and causes re-stratification.

7 Acknowledgements

I want to thank my teachers at Oslo International School for giving me technical advice for this paper. Special thanks to my Physics and Math teachers for their encouragement in exploring science outside the school curriculum. Finally, I would like to also thank Ansys Inc. for providing me educational access to the highly advanced Fluent software, which made this investigation possible.

References

[1] European Commission, Directorate-General for Climate Action, "Reducing emissions from aviation," 2025.

[2] "Hydrogen-powered aviation: A fact-based study of hydrogen technology, economics, and climate impact by 2050," technical report, Clean Sky 2 Joint Undertaking and Fuel Cells and Hydrogen 2 Joint Undertaking, Luxembourg, May 2020.

[3] Airbus, "Zeroe: Our hydrogen-powered aircraft." https://www.airbus.com/en/innovation/energy-transition/hydrogen/zeroe-our-hydrogen-powered-aircraft, 2024.

[4] R. W. Schefer, C. M. White, and J. O. Keller, "Chapter 8 – lean hydrogen combustion," in *Hydrogen and Fuel Cells: Advances in Transportation and Power*, Livermore, CA: Sandia National Laboratories, 2007. SAND2007-1524P, OSTI ID 1731098.

[5] A. Stark, "Air fuel ratio." https://x-engineer.org/air-fuel-ratio/, 2025. x-engineer.org.

[6] S. YK, "Ansys fluent tutorial n°2 — generic non-premixed combustion chamber modeling in fluent." YouTube video, Nov. 2022.

[7] U. Doll, C. Barro, M. Todino, and K. Boulouchos, "Impact of a split injection strategy on mixing, ignition and combustion behavior in premixed charge compression ignition combustion," *Fuel*, vol. 294, p. 120511, 2021.

[8] T. Cain, "Autoignition of hydrogen at high pressure," *Combustion and Flame*, vol. 111, no. 1, pp. 124–132, 1997.

[9] J. Amend, R. Lubbock, F. Ornano, and T. Povey, "Lean-burn combustor simulator for an engine-component test facility: An experimental and computational study," *Journal of Turbomachinery*, vol. 145, p. 061014, 01 2023.

[10] ANSYS, "Ansys fluent - cfd software — ansys," 2016.

[11] A. Pozarlik and J. Kok, "Experimental investigation and numerical prediction of thermo-acoustic instabilities and associated liner vibrations induced by combustion process in gas turbines," in *50th AIAA Aerospace Sciences Meeting including the New Horizons Forum and Aerospace Exposition*, (United States), pp. –, American Institute of Aeronautics and Astronautics, Jan. 2012. 50th AIAA Aerospace Sciences Meeting 2012 ; Conference date: 09-01-2012 Through 11-01-2012.

[12] Engineering ToolBox, "Higher calorific values of common fuels: Reference & data." https://www.engineeringtoolbox.com/fuels-higher-calorific-values-d_169.html.

[13] W. R. Bender, "Lean pre-mixed combustion," in *Gas Turbine Handbook*, ch. 3.2.1.2, Morgantown, WV: U.S. Department of Energy, National Energy Technology Laboratory, 2006. NETL Gas Turbine Handbook section 3.2.1.2.

[14] A. Patwardhan, "Cfd modeling of jet mixed tanks," *Chemical Engineering Science*, vol. 57, no. 8, pp. 1307–1318, 2002.

[15] P. Cardin and P. Olson, "8.11 - experiments on core dynamics," in *Treatise on Geophysics* (G. Schubert, ed.), pp. 319–343, Amsterdam: Elsevier, 2007.

[16] D. Frazier, R. Hung, M. Paley, B. Penn, and Y. Long, "Buoyancy-driven heat transfer during application of a thermal gradient for the study of vapor deposition at low pressure using an ideal gas," *Journal of Crystal Growth*, vol. 171, no. 1, pp. 288–302, 1997.

[17] M. S. Sweeney, S. Hochgreb, M. J. Dunn, and R. S. Barlow, "The structure of turbulent stratified and premixed methane/air flames i: Non-swirling flows," *Combustion and Flame*, vol. 159, no. 9, pp. 2896–2911, 2012.

A Python Code for Post-Process

```python
import pandas as pd
import numpy as np
import matplotlib.pyplot as plt
import os

# configuring the xcel file path and output folder
excel_file = 'case4_data.xlsx'
output_folder = 'Case4_Results'
os.makedirs(output_folder, exist_ok=True)

# axial positions, with the corresponding excel sheets (standardised)
axial_positions = {
    '1': 0.025,    # 25mm - Near field
    '2': 0.05,     # 50mm - Near field
    '3': 0.15,     # 150mm - Far field
    '4': 0.25,     # 250mm - Far field
    '5': 0.35      # 350mm - Far field
}

NEAR_FIELD = [0.025, 0.05]
FAR_FIELD = [0.15, 0.25, 0.35]

# extracting the data and putting it into a dataframe
xls = pd.ExcelFile(excel_file)
results = []

for sheet_name, z_m in axial_positions.items():
    z_mm = z_m * 1000

    df = pd.read_excel(excel_file, sheet_name=sheet_name)
    df.columns = df.columns.str.strip().str.lower()
    df = df[df['radius'] < 0.1].copy()
    df = df[df['h2o'] > 0.001].copy()

    mean_h2o = df['h2o'].mean()
    std_h2o = df['h2o'].std()
    SI_h2o = std_h2o / mean_h2o

    TKE = df['tke'].mean()
    TI = df['ti'].mean()

    regime = 'Near' if z_m in NEAR_FIELD else 'Far'

    results.append({
        'z_mm': z_mm,
        'z_m': z_m,
        'regime': regime,
```

```
        'SI_h2o': SI_h2o,
        'mean_h2o': mean_h2o,
        'std_h2o': std_h2o,
        'TKE': TKE,
        'TI': TI
    })

df_results = pd.DataFrame(results)

# calculating stratification gradients for near and far fields using H2O data
near_field = df_results[df_results['regime'] == 'Near'].copy()
far_field = df_results[df_results['regime'] == 'Far'].copy()

# mean strafitication gradients
gradient_near = (near_field['SI_h2o'].iloc[-1] - near_field['SI_h2o'].iloc[0]) / (near_field['z_mm'].iloc[-1] - near_field['z_mm'].iloc[0])
gradient_far = (far_field['SI_h2o'].iloc[-1] - far_field['SI_h2o'].iloc[0]) / (far_field['z_mm'].iloc[-1] - far_field['z_mm'].iloc[0])

print("="*80)
print("STRATIFICATION GRADIENT ANALYSIS")
print("="*80)
print(f"Near-field dSI/dz: {gradient_near:.6f}  m m  ")
print(f"Far-field dSI/dz:  {gradient_far:.6f}  m m  ")
print("="*80)

# plotting the results
# plot 1 : SI vs Distance
fig, ((ax1, ax2), (ax3, ax4)) = plt.subplots(2, 2, figsize=(14, 10))

ax1.plot(df_results['z_mm'], df_results['SI_h2o'], 'k-', linewidth=2)
ax1.scatter(near_field['z_mm'], near_field['SI_h2o'], s=200, c='red', marker='o', edgecolors='black', linewidths=2, label='Near-field', zorder=3)
ax1.scatter(far_field['z_mm'], far_field['SI_h2o'], s=200, c='blue', marker='s', edgecolors='black', linewidths=2, label='Far-field', zorder=3)
ax1.set_xlabel('Axial Distance [mm]', fontsize=12, fontweight='bold')
ax1.set_ylabel('Stratification Index (SI)', fontsize=12, fontweight='bold')
ax1.set_title('SI vs Distance', fontsize=13, fontweight='bold')
ax1.legend(fontsize=10)
ax1.grid(True, alpha=0.3)

# plot 2 : TKE vs Distance
ax2.plot(df_results['z_mm'], df_results['TKE'], 'g-', linewidth=2)
ax2.scatter(near_field['z_mm'], near_field['TKE'], s=200, c='red', marker='o', edgecolors='black', linewidths=2, label='Near-field',
```

```
    zorder=3)
ax2.scatter(far_field['z_mm'], far_field['TKE'], s=200, c='blue', marker
    ='s', edgecolors='black', linewidths=2, label='Far-field', zorder=3)
ax2.set_xlabel('Axial Distance [mm]', fontsize=12, fontweight='bold')
ax2.set_ylabel('TKE [m  /s  ]', fontsize=12, fontweight='bold')
ax2.set_title('TKE vs Distance', fontsize=13, fontweight='bold')
ax2.legend(fontsize=10)
ax2.grid(True, alpha=0.3)

# plot 3: SI vs TKE - Near Field
ax3.plot(near_field['TKE'], near_field['SI_h2o'], 'r-', linewidth=2)
ax3.scatter(near_field['TKE'], near_field['SI_h2o'], s=200, c='red',
    marker='o', edgecolors='black', linewidths=2, zorder=3)
ax3.set_xlabel('TKE [m  /s  ]', fontsize=12, fontweight='bold')
ax3.set_ylabel('Stratification Index (SI)', fontsize=12, fontweight='
    bold')
ax3.set_title('SI vs TKE - Near Field', fontsize=13, fontweight='bold')
ax3.grid(True, alpha=0.3)

# plot 4: SI vs TKE - Far Field
ax4.plot(far_field['TKE'], far_field['SI_h2o'], 'b-', linewidth=2)
ax4.scatter(far_field['TKE'], far_field['SI_h2o'], s=200, c='blue',
    marker='s', edgecolors='black', linewidths=2, zorder=3)
ax4.set_xlabel('TKE [m  /s  ]', fontsize=12, fontweight='bold')
ax4.set_ylabel('Stratification Index (SI)', fontsize=12, fontweight='
    bold')
ax4.set_title('SI vs TKE - Far Field', fontsize=13, fontweight='bold')
ax4.grid(True, alpha=0.3)

plt.tight_layout()
plt.savefig(f'{output_folder}/Analysis_Results.png', dpi=300)
plt.show()

# saving the results to excel files
summary = {
    'Near_field_dSI_dz': gradient_near,
    'Far_field_dSI_dz': gradient_far,
    'Initial_SI': df_results.iloc[0]['SI_h2o'],
    'Final_SI': df_results.iloc[-1]['SI_h2o']
}

summary_df = pd.DataFrame([summary])
summary_df.to_excel(f'{output_folder}/Summary.xlsx', index=False)
df_results.to_excel(f'{output_folder}/All_Data.xlsx', index=False)

print(f"\ n   Plots saved to: {output_folder}/Analysis_Results.png")
print(f"    Data saved to: {output_folder}/All_Data.xlsx")

output_excel = f'{output_folder}/Complete_Analysis_Data.xlsx'
```

```
131
132 with pd.ExcelWriter(output_excel, engine='openpyxl') as writer:
133     # Sheet 1: Summary
134     summary = {
135         'Near_field_dSI_dz': [gradient_near],
136         'Far_field_dSI_dz': [gradient_far],
137         'Initial_SI': [df_results.iloc[0]['SI_h2o']],
138         'Final_SI': [df_results.iloc[-1]['SI_h2o']]
139     }
140     summary_df = pd.DataFrame(summary)
141     summary_df.to_excel(writer, sheet_name='Summary', index=False)
142
143     # Sheet 2: All positions data
144     formatted_results = pd.DataFrame({
145         'Axial Position [mm]': df_results['z_mm'],
146         'Regime': df_results['regime'],
147         'Stratification Index (SI)': df_results['SI_h2o'],
148         'Mean H2O': df_results['mean_h2o'],
149         'Std H2O': df_results['std_h2o'],
150         'TKE [m  /s  ]': df_results['TKE'],
151         'Turbulence Intensity [%]': df_results['TI']
152     })
153     formatted_results.to_excel(writer, sheet_name='All_Positions', index
    =False)
154
155     # Individual sheets for each position
156     for idx, row in df_results.iterrows():
157         position_data = pd.DataFrame({
158             'Parameter': ['Axial Position [mm]', 'Regime', '
    Stratification Index (SI)',
159                           'Mean H2O', 'Std H2O', 'TKE [m  /s  ]', '
    Turbulence Intensity [%]'],
160             'Value': [row['z_mm'], row['regime'], row['SI_h2o'],
161                       row['mean_h2o'], row['std_h2o'], row['TKE'], row['
    TI']]
162         })
163         sheet_name = f'z={int(row["z_mm"])}mm'
164         position_data.to_excel(writer, sheet_name=sheet_name, index=
    False)
165
166 print(f"\ n   Plots saved to: {output_folder}/Analysis_Results.png")
167 print(f"    All data saved to: {output_excel}")
```